

A Deconfounding Approach to Climate Model Bias Correction

Wentao Gao¹, Jiuyong Li¹, Debo Cheng¹, Lin Liu¹, Jixue Liu¹, Thuc Duy Le¹, Xiaojing Du¹,
Xiongren Chen¹, Yanchang Zhao², Yun Chen²

¹University of South Australia

²Commonwealth Scientific and Industrial Research Organisation(CSIRO)
gaowy014@mymail.unisa.edu.au

Abstract

Global Climate Models (GCMs) are crucial for predicting future climate changes by simulating the Earth systems. However, GCM outputs exhibit systematic biases due to model uncertainties, parameterization simplifications, and inadequate representation of complex climate phenomena. Traditional bias correction methods, which rely on historical observation data and statistical techniques, often neglect unobserved confounders, leading to biased results. This paper proposes a novel bias correction approach to utilize both GCM and observational data to learn a factor model that captures multi-cause latent confounders. Inspired by recent advances in causality based time series deconfounding, our method first constructs a factor model to learn latent confounders from historical data and then applies them to enhance the bias correction process using advanced time series forecasting models. The experimental results demonstrate significant improvements in the accuracy of precipitation outputs. By addressing unobserved confounders, our approach offers a robust and theoretically grounded solution for climate model bias correction.

Introduction

Global Climate Models (GCMs), such as those developed by the Coupled Model Intercomparison Project phase 6 (CMIP6) (Eyring et al. 2016), are vital tools for predicting future climate changes. These models simulate the physical and chemical processes of the Earth systems—including the atmosphere, oceans, land, and ice—to provide detailed climate forecasts. Despite significant advancements in GCM, their output still exhibits systematic biases. These biases primarily come from uncertainties within the models, simplifications in parameterization processes, and inadequate representations of complex climate phenomena (Mouatadid et al. 2023). For instance, processes such as cloud formation, precipitation, radiation, and convection are often simplified into parameterization formulas in GCMs, which may not accurately reflect real-world conditions, thus leading to biases. Consequently, (Lafferty and Srivier 2023) highlighted that bias corrections were particularly crucial for near-term precipitation projections, especially in cases where observational data are inconsistent with GCMs output.

To enhance the reliability and accuracy of GCM outputs, numerous bias correction techniques, ranging from simple linear scaling to advanced quantile mapping, have been proposed to modify GCM outputs and align them more closely with actual observations (Casanueva et al. 2020; Chen et al. 2013; Dowdy 2020; Enayati et al. 2020; Feigenwinter et al. 2018; Heo et al. 2019; Lafon et al. 2013; Maraun 2016; Mehrotra, Johnson, and Sharma 2018; Miao et al. 2016; Nahar, Johnson, and Sharma 2018; Piani, Haerter, and Coppola 2010; Smitha et al. 2018; Teutschbein and Seibert 2012a; Wu et al. 2022b). These methods typically rely on historical observation data and statistical approaches to adjust climate model outputs and correct systematic errors (Maraun and Widmann 2018).

However, these traditional methods have been found to inflate simulated extremes, raising concerns about their use in climate change applications where extremes are significant, such as drought and flooding (Huang, Hall, and Berg 2014; Pastén-Zapata et al. 2020). Another major limitation of most bias correct methods is their assumption that all relevant factors are known and observable, which is unrealistic in practical applications. Climate systems are complex and include many factors that may not be fully observed, such as microclimate effects, regional climate characteristics, and anthropogenic influences. These potential unobserved (confounding) factors dynamically impact time series forecast. However, since they cannot be fully observed, they are frequently overlooked by current bias correction methods. This overlook limits the potential of most existing methods in bias correction.

To deal with the challenge of extreme conditions, the study by (Nivron et al. 2024) incorporates advanced time series forecasting models into the bias correction of extreme weather events, such as heatwaves, by considering the bias correction as a time-indexed regression model with stochastic output. This provides a new perspective: adapting time series forecasting models to bias correction can improve model performance. However, although advanced models have shown significant potential in time series forecasting (Zhou et al. 2021; Wu et al. 2022a, 2023a; Wang et al. 2024), particularly in climate forecasting (Bi et al. 2023; Wu et al. 2023b), they typically overlook the existence of unobserved confounding factors, which leads to biased results.

In the field of causal inference with time series, recent

| Time period | History | Current | Future |
|-------------------------|--|--|----------------------------------|
| | $[t - h - w - 1, \dots, t - w]$ | $[t, t + 1, \dots, t + k + 1]$ | |
| GCM (G) | \mathbf{X}_t^G (humidity, pressure, ...) | \mathbf{A}_t^G (humidity, pressure, ...) | \mathbf{Y}_t^G (precipitation) |
| Observations (O) | \mathbf{X}_t^O (humidity, pressure, ...) | \mathbf{A}_t^O (humidity, pressure, ...) | \mathbf{Y}_t^O (precipitation) |

Table 1: A description of data variables for GCM and observations.

studies have started addressing the challenge of unobserved confounders in predicting the potential outcomes of treatments in time series data. Instead of assuming unconfoundedness (Pearl 2000), these studies operate under a weaker assumption that only multi-cause confounders exist (Bica, Alaa, and van der Schaar 2020; Wang and Blei 2019; Li et al. 2024; Cheng et al. 2023; Xu et al. 2023). A variable is said to be a confounder if it is a common cause of both the treatment and the outcome (Pearl 2009). For example, in the Directed Acyclic Graph (DAG) shown in Figure 1(a), the confounder \mathbf{X} affects both the treatment \mathbf{A} and outcome Y . In our bias correction problem, precipitation output is always treated as the outcome, and other related climate variables are treated as treatment variables. The most common method for predicting potential outcomes is to use all treatment variables. However, neglecting unobserved multi-cause confounders \mathbf{Z} , such as large-scale atmospheric circulation patterns or oceanic processes, can lead to simultaneous effects on various climate variables, including precipitation. These multi-cause confounders make it possible to apply current research outcomes to bias correction in GCM.

Inspired by the work of (Bica, Alaa, and van der Schaar 2020), in this paper, we propose a deconfounding bias correction method. It is important to note that estimating hidden confounders in climate bias correction is much more complex. This increased complexity arises not only from the intricate nature of hidden confounders in climate science but also because these confounders need to be inferred from GCM and observation data.

Our contribution can be summarized as the following:

1. We use causality to identify and understand unobserved confounders, allowing us to obtain unbiased outcome in the presence of multi-cause confounders. By identifying latent confounders through constructing a factor model over time, our approach can capture these unobserved factors, resulting in unbiased outcomes.
2. We develop a two-phase algorithm: Deconfounding and Correction. The Deconfounding Bias Correction (BC) factor model captures the confounders from both Global Climate Model (GCM) output data and observational data, and the correction model uses these confounders as additional information for the bias correction task. Inspired by the TSD (Time Series Deconfounder) (Bica, Alaa, and van der Schaar 2020), our method extend to GCM and observation data.

Problem Formulation

As shown in Table 1, let the random variable \mathbf{V} represent the set of climate variables, such as humidity, temperature, pressure, precipitation and others. Among these variables, Y denote the outcome of interest, for example, precipitation. In our problem setting, because we will use both historical and current data of these variables, to avoid confusion, \mathbf{X}_t represent historical version of $\mathbf{V} \setminus Y$. \mathbf{A}_t represent current version of $\mathbf{V} \setminus Y$.

These variables are collected from two sources: Global climate models (GCMs) and observations. Moreover, we use \mathbf{X}_t^G and \mathbf{A}_t^G to represent historical and current variables of the GCM data respectively, while \mathbf{X}_t^O and \mathbf{A}_t^O for historical and current variables. The outcome from GCMs and observations are denoted as Y_t^G and Y_t^O respectively.

The data for a location, also known as the location trajectory, consist of realizations of the previously described random variables $\{\mathbf{x}_t^G, \mathbf{a}_t^G, y_t^G, \mathbf{x}_t^O, \mathbf{a}_t^O, y_t^O\}$. Let $y(\bar{\mathbf{a}}_t)$ represent the potential outcome (precipitation), which could be either factual or counterfactual, for each possible treatment course $\bar{\mathbf{a}}_t$, where $\bar{\mathbf{a}}_t = (\mathbf{a}_1, \dots, \mathbf{a}_t)$. Consequently, we have $y^G(\bar{\mathbf{a}}_t)$ and $y^O(\bar{\mathbf{a}}_t)$. The concept of potential outcomes allows us to consider what the outcome y would be under different treatment scenarios, which is essential for causal inference (Rubin 1974).

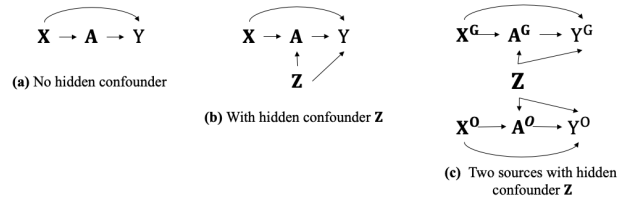


Figure 1: Summary causal graphs under three conditions: (a) No hidden confounder, (b) With hidden confounder \mathbf{Z} , (c) Two sources with hidden confounder \mathbf{Z}

To correct future k steps precipitation bias $\Delta Y = Y^O - Y^G$ which is the difference between observational precipitation y^O and GCM output precipitation y^G , a common way is to use all data to obtain a regression model (Nivron et al. 2024) which can be represented by Figure 1(a). However, the existence of hidden confounders (e.g. unobserved atmospheric and oceanic circulation) will result in biased result. To address the issue of hidden confounders in time series data, (Bica, Alaa, and van der Schaar 2020) have developed a method, assuming the presence of multi-cause hidden con-

founders \mathbf{Z} , as shown in the Figure 1(b).

However, no attempt has been made to adapt their work to bias correction, including bias correction for climate models. In this paper, we extend the work for the bias correction problem as shown in the Figure 1(c) which make the most of information we have. We assume that hidden variables \mathbf{Z} affect both GCM and observations. Learning \mathbf{Z} , we would estimate the potential outcome in observations for each location conditional on the location history of covariates $\bar{\mathbf{X}}_t^O = (\mathbf{X}_1^O, \dots, \mathbf{X}_t^O) \in \mathcal{X}_t^O$, treatments $\bar{\mathbf{A}}_t^O = (\mathbf{A}_1^O, \dots, \mathbf{A}_t^O) \in \mathcal{A}_t^O$ and confounders $\bar{\mathbf{Z}}_t = (\mathbf{Z}_1, \dots, \mathbf{Z}_t) \in \mathcal{Z}_t$:

$$\mathbf{E} [\mathbf{Y}^O(\bar{\mathbf{a}}_{\geq t}^O) \mid \bar{\mathbf{A}}_{t-1}^O, \bar{\mathbf{X}}_t^O, \bar{\mathbf{Z}}_t]$$

Proposed method

The existence of confounders can result in the obtained association among $\mathbf{X}, \mathbf{A}, \mathbf{Y}$ not accurately representing the true relationships, potentially leading to biased results. To solve this, we (1) input the climate model data into the Deconfounding Bias Correction (BC) factor model to obtain the multi-cause hidden confounder which is essential for bias correction (we call this step 'Deconfounding'). Then (2) we use a hidden multicause confounder as a bias source, combine it with observational data, building a precipitation correction model to help the climate model to have a better estimate of future output (we call this step 'Correction').

Deconfounding

To address the challenge of deconfounding time series data with time varying latent confounder, (Bica, Alaa, and van der Schaar 2020) proposed the Time Series Deconfounder (TSD), which extends the deconfounder methodology introduced by (Wang and Blei 2019) to the time series domain. The fundamental principle of the TSD is that It utilizes factor model to infer substitutes for hidden confounders as treatments.

The goal of this part is to generalize the factor model proposed by (Bica, Alaa, and van der Schaar 2020) to a Deconfounding BC factor model for bias correction. This extension aims to extend the Time Series Deconfounder to a complex time series setting of two sources.

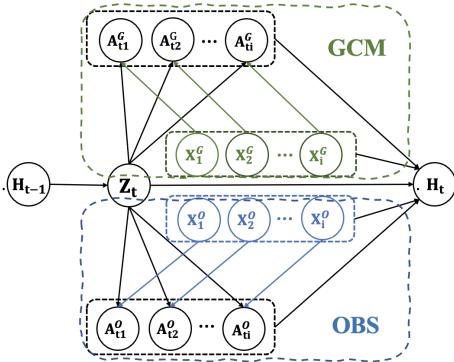


Figure 3: Double source, i denote as the total number of climate variables.

Deconfounding BC factor model To extend time series deconfounder (Bica, Alaa, and van der Schaar 2020) to bias correction, We propose an enhanced multi-source factor model specially for this task, termed the Deconfounding BC factor model.

For single source data, the unobserved confounder affects $\mathbf{X}, \mathbf{A}, \mathbf{Y}$ from one source, allowing us to infer the sequence of unobserved confounders $\mathbf{z}_t = g(\bar{\mathbf{h}}_{t-1})$, where $\bar{\mathbf{h}}_{t-1} = \{\bar{\mathbf{a}}_{t-1}, \bar{\mathbf{x}}_{t-1}, \bar{\mathbf{z}}_{t-1}\}$ is the realization of $\bar{\mathbf{H}}_{t-1}$. Specifically, factorization can be expressed as follows:

$$p(a_{t1}, \dots, a_{tk} \mid \mathbf{z}_t, \mathbf{x}_t) = \prod_{j=1}^k p(a_{tj} \mid \mathbf{z}_t, \mathbf{x}_t).$$

To extend this model for multi-source data, consider both GCM and Observations. The unobserved confounder will affect $\mathbf{X}, \mathbf{A}, \mathbf{Y}$ in both sources, allowing us to infer the sequence of unobserved confounders $\mathbf{z}_t = g(\bar{\mathbf{h}}_{t-1})$ that can be used to render both source treatments conditionally independent, where $\bar{\mathbf{h}}_{t-1} = \{\bar{\mathbf{h}}_{t-1}^O, \bar{\mathbf{h}}_{t-1}^G\}$ is the realization of $\bar{\mathbf{H}}_{t-1}$. Specifically, the factorization for the multi-source scenario can be expressed as follows:

$$p(a_{t1}^O, \dots, a_{tk}^O \mid \mathbf{z}_t, \mathbf{x}_t^O) = \prod_{j=1}^k p(a_{tj}^O \mid \mathbf{z}_t, \mathbf{x}_t^O),$$

$$p(a_{t1}^G, \dots, a_{tk}^G \mid \mathbf{z}_t, \mathbf{x}_t^G) = \prod_{j=1}^k p(a_{tj}^G \mid \mathbf{z}_t, \mathbf{x}_t^G).$$

It allows us to infer the sequence of latent variables \mathbf{Z} that can be used to render the treatments conditionally independent with the observed location covariates \mathbf{x}_t . As in one location, the same confounders \mathbf{Z} will affect both GCM and observations. In this case, the \mathbf{Z} we learned should render treatments in both GCM and observational data.

Since the structure of the factor model depends on causality, which relies on the assumptions listed below.

assumption 1. Consistency. If $\bar{A}_{\geq t} = \bar{a}_{\geq t}$, then the potential outcomes for following the treatment $\bar{a}_{\geq t}$ is the same as the factual outcome $Y(\bar{a}_{\geq t}) = Y$.

assumption 2. Positivity (Overlap): if $P(\bar{\mathbf{A}}_{t-1} = \bar{\mathbf{a}}_{t-1}, \bar{\mathbf{X}}_t = \bar{\mathbf{x}}_t) \neq 0$ then $P(A_t = a_t \mid \bar{\mathbf{A}}_{t-1} = \bar{\mathbf{a}}_{t-1}, \bar{\mathbf{X}}_t = \bar{\mathbf{x}}_t) > 0$ for all a_t .

assumption 3. Sequential Single Strong Ignorability

$\mathbf{Y}(\bar{\mathbf{a}}_{\geq t}) \perp\!\!\!\perp \mathbf{A}_{tj} \mid \mathbf{X}_t, \bar{\mathbf{H}}_{t-1}$, for all $t \in \{0, \dots, T\}$, and for all $j \in \{1, \dots, k\}$.

Next, we provide a theoretical analysis for the soundness of the learned \mathbf{Z}_t by introducing the concept of sequential Kallenberg construction (Bica, Alaa, and van der Schaar 2020), as follows.

Definition 1. Sequential Kallenberg construction At timestep t , we say that the distribution of assigned causes $(\mathbf{A}_{t1}^G, \dots, \mathbf{A}_{tk}^G), (\mathbf{A}_{t1}^O, \dots, \mathbf{A}_{tk}^O)$ admits a sequential Kallenberg construction from the random variables $\mathbf{Z}_t = g(\bar{\mathbf{H}}_{t-1}^O, \bar{\mathbf{H}}_{t-1}^G)$ and $\mathbf{X}_t^O, \mathbf{X}_t^G$ if there exist measurable functions $f_{tj}^O : \mathbf{Z}_t^O \times \mathbf{X}_t^O \times [0, 1] \rightarrow \mathcal{A}_j^O$ and $f_{tj}^G : \mathbf{Z}_t^G \times \mathbf{X}_t^G \times$

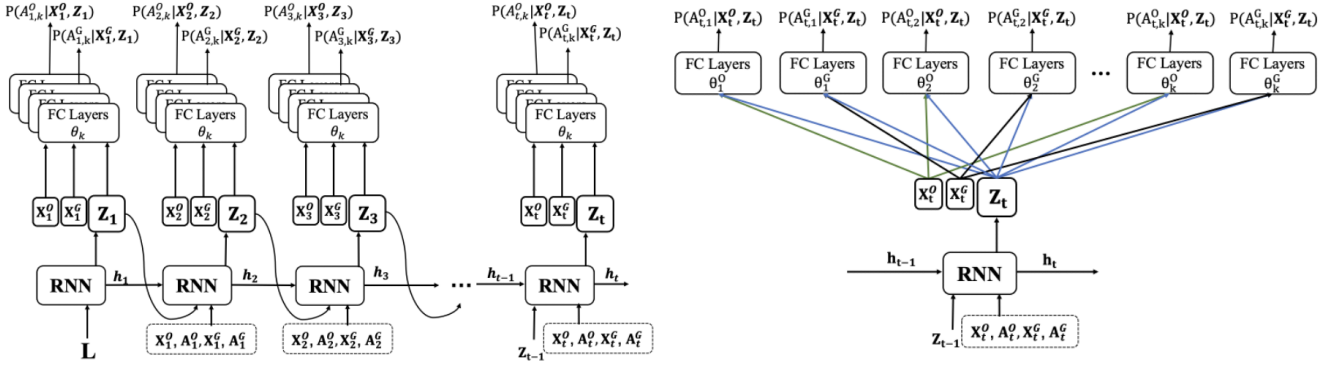


Figure 2: Deconfounding BC factor model

$[0, 1] \rightarrow A_j^G$ and random variables $U_{tj}^O, U_{tj}^G \in [0, 1]$, with $j = 1, \dots, k$ such that:

$$A_{tj}^O = f_{tj}^O(\mathbf{Z}_t, \mathbf{X}_t^O, U_{tj}^O),$$

$$A_{tj}^G = f_{tj}^G(\mathbf{Z}_t, \mathbf{X}_t^G, U_{tj}^G),$$

where U_{tj}^O, U_{tj}^G marginally follow $\text{Uniform}[0, 1]$ and jointly satisfy:

$$(U_{t1}^O, \dots, U_{tk}^O) \perp Y^O(\bar{\mathbf{a}}_{\geq t}^O) \mid \mathbf{Z}_t, \mathbf{X}_t^O, \bar{\mathbf{H}}_{t-1}^O,$$

$$(U_{t1}^G, \dots, U_{tk}^G) \perp Y^G(\bar{\mathbf{a}}_{\geq t}^G) \mid \mathbf{Z}_t, \mathbf{X}_t^G, \bar{\mathbf{H}}_{t-1}^G,$$

for all $\bar{\mathbf{a}}_{\geq t}^O$ and $\bar{\mathbf{a}}_{\geq t}^G$.

We present the following theorem to guarantee that the learned \mathbf{Z}_t can serve as a substitute for the multi cause hidden confounders.

theorem 1. The soundness of the learned \mathbf{Z}_t If at every timestep t , the two distribution of assigned causes $(\mathbf{A}_{t1}^G, \dots, \mathbf{A}_{tk}^G)$, $(\mathbf{A}_{t1}^O, \dots, \mathbf{A}_{tk}^O)$ admit a Kallenberg construction from $\mathbf{Z}_t = g(\bar{\mathbf{H}}_{t-1}^O, \bar{\mathbf{H}}_{t-1}^G)$ and $\mathbf{X}_t^O, \mathbf{X}_t^G$ separately, then the learned \mathbf{Z}_t can serve as a substitute for the multi cause hidden confounders.

Theorem 1 shows that the latent variables \mathbf{Z}_t are inferred using the fact causes $(A_{t1}^G, \dots, A_{tk}^G)$ and $(A_{t1}^O, \dots, A_{tk}^O)$ are jointly independent given \mathbf{Z}_t and $\mathbf{X}_t^G, \mathbf{X}_t^O$ as shown in Figure 3. The result means that, at each timestep, for both sources, the variable $\bar{\mathbf{X}}_t, \bar{\mathbf{Z}}_t, \bar{\mathbf{A}}_{t-1}$ contain all of the dependencies between the potential outcomes $\mathbf{Y}(\bar{\mathbf{a}}_{\geq t})$ and the assigned causes \mathbf{A}_t . See the Appendix for the full proof.

Then for both sources we have,

$$\mathbf{E}[Y(\bar{\mathbf{a}}_{\geq t}) \mid \bar{\mathbf{A}}_{t-1}, \mathbf{X}_t, \bar{\mathbf{Z}}_t] = \mathbf{E}[Y \mid \bar{\mathbf{a}}_{\geq t}, \bar{\mathbf{A}}_{t-1}, \mathbf{X}_t, \bar{\mathbf{Z}}_t].$$

This equation implies that the potential outcome can be represented by $\mathbf{E}[Y \mid \bar{\mathbf{a}}_{\geq t}, \bar{\mathbf{A}}_{t-1}, \mathbf{X}_t, \bar{\mathbf{Z}}_t]$. Therefore, our estimate of the potential outcome is unbiased given the previous treatments, current covariates, and latent variables. This unbiasedness is crucial for making valid inferences about causal effects.

Then, we will show how to implement in practical. The joint distribution of all collected T time steps in our enhanced Deconfounding BC Factor Model can be formulated as follows:

$$p(\theta_{1:k}^G, \bar{\mathbf{x}}_T^G, \bar{\mathbf{z}}_T, \bar{\mathbf{a}}_T^G) =$$

$$p(\theta_{1:k}^G) p(\bar{\mathbf{x}}_T^G) \prod_{t=1}^T p(\mathbf{z}_t \mid \bar{\mathbf{h}}_{t-1}) \prod_{j=1}^k p(\mathbf{a}_{tj}^G \mid \mathbf{z}_t, \mathbf{x}_t^G, \theta_j^G),$$

$$p(\theta_{1:k}^O, \bar{\mathbf{x}}_T^O, \bar{\mathbf{z}}_T, \bar{\mathbf{a}}_T^O) =$$

$$p(\theta_{1:k}^O) p(\bar{\mathbf{x}}_T^O) \prod_{t=1}^T p(\mathbf{z}_t \mid \bar{\mathbf{h}}_{t-1}) \prod_{j=1}^k p(\mathbf{a}_{tj}^O \mid \mathbf{z}_t, \mathbf{x}_t^O, \theta_j^O),$$

where $\theta_{1:k}^O$ and $\theta_{1:k}^G$ are the model parameters. The treatment distributions $p(\bar{\mathbf{a}}_T^O)$ and $p(\bar{\mathbf{a}}_T^G)$ are the corresponding marginal distributions.

In practical applications, as shown figure 2, we need to build a model to get \mathbf{Z} with predicting treatments as the constraint. To manage time-varying treatments $\mathbf{A}^G, \mathbf{A}^O$, we follow a pragmatic approach utilizing a recurrent neural network (RNN) with multitask output for implementation.

The recurrent model infers the latent variables \mathbf{Z}_t based on location history:

$$\mathbf{Z}_1 = \text{RNN}(\mathbf{L}),$$

$$\mathbf{Z}_t = \text{RNN}(\mathbf{Z}_{t-1}, \mathbf{X}_{t-1}^G, \mathbf{A}_{t-1}^G, \mathbf{X}_{t-1}^O, \mathbf{A}_{t-1}^O, \mathbf{L}),$$

where \mathbf{L} consists of randomly initialized trainable parameters. Note that in each time step t , the assignments $\mathbf{A}_t^O = [A_{t1}^O, \dots, A_{tk}^O]$ and $\mathbf{A}_t^G = [A_{t1}^G, \dots, A_{tk}^G]$ are conditionally independent given $\mathbf{Z}_t, \mathbf{X}_t^O$ and $\mathbf{Z}_t, \mathbf{X}_t^G$ separately:

$$A_{tj}^G = \text{FC}(\mathbf{X}_t^G, \mathbf{Z}_t, \theta_j^G),$$

$$A_{tj}^O = \text{FC}(\mathbf{X}_t^O, \mathbf{Z}_t, \theta_j^O),$$

for all j and t , where θ_j^G and θ_j^O are the parameters of the fully connected layers. Using this as multitask output, treatments is conditionally independent given $\mathbf{X}_t, \mathbf{Z}_t$ for both sources, this can be ensured by inferring each treatment A^G or A^O as different tasks with only $\mathbf{X}_t^G, \mathbf{Z}_t$ or $\mathbf{X}_t^O, \mathbf{Z}_t$, if we condition on $\mathbf{X}_t^G, \mathbf{Z}_t$ or $\mathbf{X}_t^O, \mathbf{Z}_t$, they are conditionally independent.

Training The factor model is trained using gradient descent methods on the observational and GCM dataset. The architecture leverages the dependencies between multiple treatments and the location history to infer the latent variables.

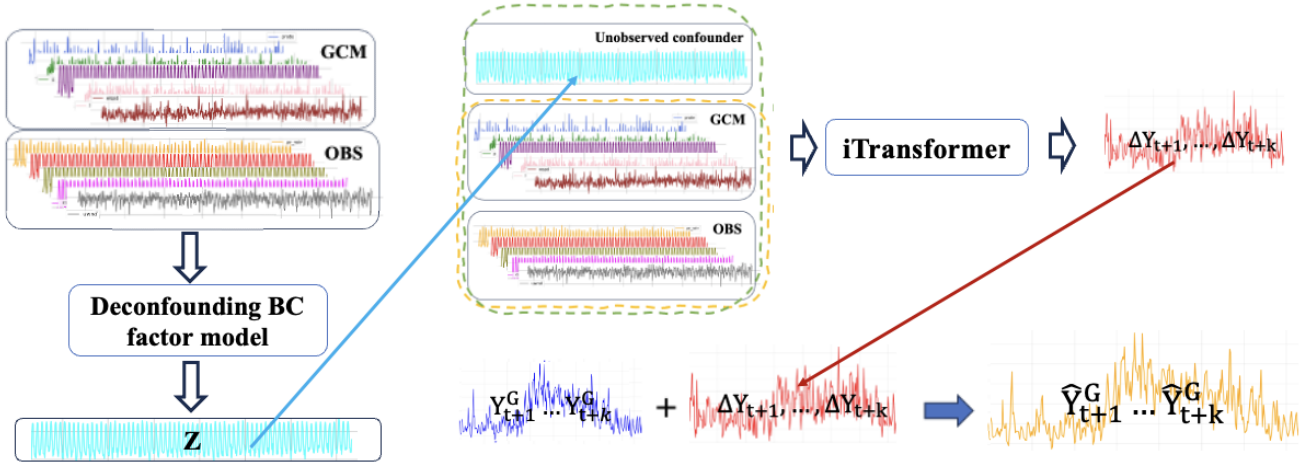


Figure 4: The overall process of Deconfounding Bias Correction. The process begins with the Deconfounding BC factor model, which extracts a latent variable \mathbf{Z} from both Global Climate Model (GCM) data and observational (OBS) data. This latent variable represents unobserved confounders that affect both datasets. The iTransformer then utilizes this latent variable \mathbf{Z} to generate correction terms for the GCM predictions, adjusting for bias and producing more accurate future climate predictions. This general process ensures that the GCM outputs are corrected for taking into account unobserved confounders.

Correction

After obtaining hidden multi-cause confounders \mathbf{Z} from both GCM and observational data in one area. In our problem formulation, we aim to correct the bias between Y^G and Y^O while considering unobserved confounders. A key question is how to utilize this information for bias correction. Advanced time series forecasting models such as iTransformer (Liu et al. 2024) have demonstrated significant potential in capturing temporal information, and integrating these models into our bias correction approach promises substantial improvements.

We propose to use probability model for bias correction. As Figure 4 shown, we build a prediction model based on the observational data and the multi-cause confounder \mathbf{Z} to predict future precipitation.

The probability model employed in is to obtain predicted ΔY . The probability model can theoretically be any time series prediction model capable of generating samples from $P_\theta(\Delta Y_{t+k} | \mathbf{A}^G, \mathbf{A}^O, \mathbf{Z})$, possessing an explicit likelihood form, and utilizing the constructed training data for this purpose. For instance, a linear regression model may serve as the forecasting model. However, due to its inherent assumption of independence among the elements of ΔY_{t+k} , it is likely to result in a poor fit.

To perform well in such a forecasting task. We choose the state of art forecasting model iTransformer (Liu et al. 2024). The reason why we choose this model is: first, its performance in long-term forecasting is great. second, it is a simple model that is an inverted transformer designed for time series. More details about iTransformer can be found in the Appendix.

After we get the ΔY_{t+k} , We can obtain our corrected

GCM output with:

$$\{\hat{Y}_{t+1}^G, \hat{Y}_{t+2}^G, \dots, \hat{Y}_{t+k}^G\} = \{Y_{t+1}^G + \Delta Y_{t+1}, \\ Y_{t+2}^G + \Delta Y_{t+2}, \dots, Y_{t+k}^G + \Delta Y_{t+k}\}$$

Experiments and results

The objectives of the experiments are as follows: 1) Use synthetic data sets to evaluate the correctness of the latent confounder captured by our deconfounding method. 2) Build a correction model to correct precipitation predictions made by the climate model. Implementation code will be given later.

Experiments on Synthetic Data

To assess the effectiveness of our deconfounding method proposed in this paper, we conducted experiments using synthetic data in which we use predictive analysis to assess the influence of hidden confounders. Validation with real-world data is challenging because the true impact of hidden confounding cannot be precisely determined (Wang and Blei 2019).

Simulated dataset To maintain the generality of the simulation process, we propose generating a dataset using a two-source autoregressive model based on the causal summary graph shown in Figure 1(c). At each timestep t , we simulate time-varying covariates X_t from two sources (X_t^{source1} and X_t^{source2}), along with a multi-cause hidden confounder Z_t . A detailed description of the data generation process is provided in the Appendix.

We create datasets that include 500 locations, 3650 timesteps, and $k = 3$ covariates and treatments. To introduce time dependencies, we assign $p = 5$. Each dataset is

divided into an 80/10/10 split for training, validation, and testing purposes, respectively.

Our method’s effectiveness relies on two key points. First, the inferred latent variable \mathbf{Z} must, along with \mathbf{X} , accurately predict the treatment \mathbf{A} . This ensures that \mathbf{A} is conditionally independent given \mathbf{Z} and \mathbf{X} . Second, and most importantly, our method aims to learn the latent confounder \mathbf{Z} . If the inferred \mathbf{Z} closely matches or has a similar distribution to the simulation-generated \mathbf{Z} , it demonstrates that our method successfully captures the true latent confounders.

The theory posits that using inferred latent variables as substitutes for hidden confounders can yield unbiased outcomes, leveraging the factor model’s ability to accurately capture the distribution of the assigned causes. If the multi-layer output aligns well with the generated treatment, we can assert that our method effectively captures the treatment and ensures these treatments are conditionally independent when conditioned on covariates and confounders, as previously discussed.

To validate this, we performed a predictive check. The mean squared error (MSE) for the assigned treatment is 0.06157, indicating the effectiveness of our method in capturing treatments. Additionally, we compared the inferred \mathbf{Z} with the simulation-generated \mathbf{Z} . The resulting MSE is 0.00187. This further demonstrates the effectiveness of our method in learning latent confounders.

Case study: South Australia

In a bias correction (BC) process, data from climate models are compared to actual observations (or their proxies, like reanalysis products) to adjust for biases. Since global climate models (GCMs) usually have a lower resolution compared to observations or reanalysis reference data, BC often involves downscaling the resolution of GCMs. We adopt this methodology as well. For the climate model data, we selected the 15 initial condition runs from the Institut Pierre-Simon Laplace (IPSL) climate model as part of the sixth Coupled Model Intercomparison Project (CMIP6) historical experiment. The data, which is available on a monthly basis, includes climate variables such as tmax (maximum temperature 2 meters above the surface) and prate (precipitation rate), with our bias correction efforts centered on prate.

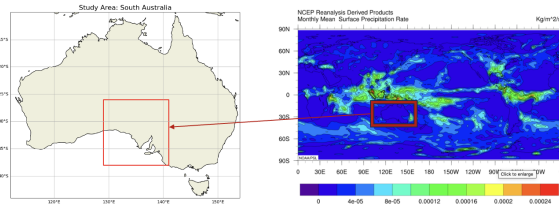


Figure 5: Study Area: South Australia (Latitude: -35.0° to -28.0° , Longitude: 129.0° to 141.0°)

The IPSL¹ model is run at a 250km nominal resolution and is not re-gridded. We selected the closest geographical

¹IPSL data portal: <https://aims2.llnl.gov/search/cmip6/>

point to South Australia for the case study, covering the period from 1948 to 2014.

For observational reference data, NCEP-NCAR Reanalysis², provided by the National Oceanic and Atmospheric Administration (NOAA), is utilized. The dataset encompasses the same variables as the IPSL model (e.g., tmax & prate). NCEP-NCAR reanalysis data is available at a monthly frequency, covering the period from 1948 to 2014, with a global resolution of 2.5 degrees in both the latitudinal and longitudinal directions, and has not been re-gridded. The nearest geographical point to South Australia was selected.

This research concentrates on bias correction of the precipitation rate (prate) to improve the accuracy of precipitation predictions.

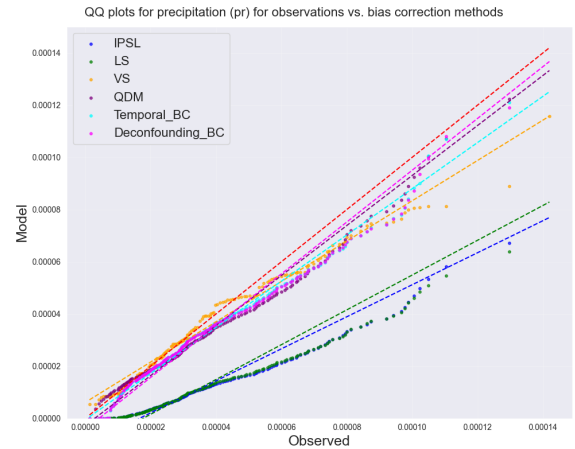


Figure 6: QQ plots for South Australia, 1993-2014, comparing observed precipitation (X-axis) with precipitation estimated by bias correction (BC) methods (Y-axis). The closer the alignment to the red line, the better the performance.

Data Preprocessing We extracted and converted climate data from 1948 to 2014 for the South Australia region as shown in Figure 5. The data, originally in NetCDF format, were transformed into CSV files for further processing. Subsequently, we split the data into a training period (1948-1992) and a testing period (1993-2014). The IPSL dataset contains 30 initial conditions; to generalize our model, we selected 15 initial conditions for the experiment. In this paper, we present results from three of these initial conditions (r5i1p1f1, r6i1p1f1 and r7i1p1f1) along with their average results. Complete results can be found in the Appendix.

Experiment settings To evaluate our proposed method, we compare our methods with several bias correction baseline methods, including linear scaling (Teutschbein and Seibert 2012b), variance scaling (Teutschbein and Seibert 2012b), quantile mapping (Cannon, Sobie, and Murdock 2015), quantile delta mapping (Tong et al. 2021) and Temporal BC (Nivron et al. 2024) methods. Implementation details of baselines are introduced in Appendix. The metric we

²NCEP-NCAR data portal: <https://psl.noaa.gov/data/gridded/data.ncep.reanalysis.html>

| Method | Exp 1 | Exp 2 | Exp 3 | Average |
|------------------------|------------------------|-------------------------|-------------------------|-------------------------|
| | MSE / MAE | MSE / MAE | MSE / MAE | MSE / MAE |
| IPSL | 0.076 / 0.217 | 0.0507 / 0.1731 | 0.0191 / 0.1059 | 0.0486 / 0.1653 |
| Linear Scaling | 0.0373 / 0.148 | 0.0423 / 0.1587 | 0.0379 / 0.1471 | 0.0392 / 0.1512 |
| Variance Scaling | 0.0055 / 0.0541 | 0.0072 / 0.0614 | 0.0113 / 0.0782 | 0.0080 / 0.0646 |
| Quantile Mapping | 0.0479 / 0.166 | 0.0413 / 0.1535 | 0.0473 / 0.1637 | 0.0455 / 0.1611 |
| Quantile Delta Mapping | 0.0347 / 0.141 | 0.0320 / 0.1348 | 0.0140 / 0.0885 | 0.0270 / 0.1211 |
| Temporal BC | 0.0042 / 0.0412 | 0.0047 / 0.0327 | 0.0049 / 0.0411 | 0.0046 / 0.0383 |
| Deconfounding BC | 0.0018 / 0.0175 | 0.0016 / 0.01615 | 0.0025 / 0.01529 | 0.0020 / 0.01632 |

Table 2: Comparison of Bias Correction Methods Across Multiple Experimental Conditions. Exp 1, Exp 2, and Exp 3 correspond to the climate model outputs based on r5i1p1f1, r6i1p1f1, and r7i1p1f1, respectively. For Temporal BC and Deconfounding BC, a 36-month history input sequence length and a 3-month future output sequence length were chosen. Bolded values represent the best results in each experiment.

| Metric | Obs | Exp1 (r5i1p1f1) | | Exp2 (r6i1p1f1) | | Exp3 (r7i1p1f1) | |
|--------|---------|-----------------|-----------|-----------------|-----------|-----------------|-----------|
| | | With Z | Without Z | With Z | Without Z | With Z | Without Z |
| MSE | 0.00848 | 0.001771 | 0.004275 | 0.001632 | 0.002162 | 0.002523 | 0.002995 |
| MAE | 0.0186 | 0.01751 | 0.03346 | 0.01615 | 0.01840 | 0.01529 | 0.02323 |

Table 3: Comparison of Correction Model Results With and Without Latent Confounder Across Multiple Experimental Conditions. Bolded values represent the best results in each experiment.

are using to compare the performance is the Mean Squared Error (MSE) and the Mean Absolute Error (MAE).

Results

Table 2 illustrates the three-step-ahead predictions using our deconfounding bias correction method on the dataset with different GCM initial settings. After applying the deconfounding step and augmenting the dataset with substitutes for the hidden confounders, we evaluated the performance of various bias correction methods using MSE and MAE. The results in Table 2 support the effectiveness of the Deconfounding BC method, which consistently achieves the lowest MSE and MAE across all experimental conditions. This indicates its superior performance in reducing prediction errors and aligning closely with the observed data.

The QQ plots (Figure 6) reveal that among the evaluated bias correction methods, Deconfounding BC shows the closest alignment with the red dashed line ($y=x$) across the entire range of observed precipitation values. This indicates that Deconfounding BC is the most effective in accurately capturing the observed precipitation levels, outperforming other methods in reducing biases and providing reliable predictions.

Figure 7 presents box plots of monthly precipitation values for South Australia using different bias correction methods, with ‘obs’ representing the observed (real) values. Among the methods compared, Deconfounding BC stands out for its effectiveness in bias correction. The box plot for Deconfounding BC shows a median and distribution range that closely match the observed values, indicating that this method captures the variability and distribution of real precipitation data more accurately than other methods.

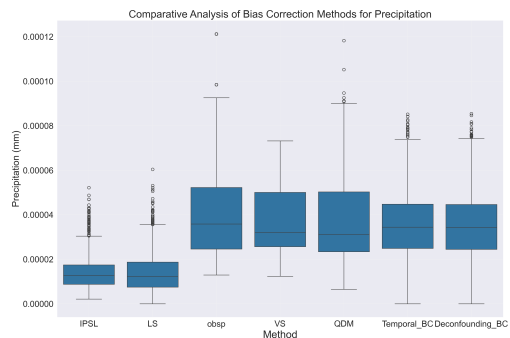


Figure 7: Box plots of monthly precipitation values for South Australia using different bias correction methods.

Ablation Study

To demonstrate that the latent confounder learned by our Deconfounding BC factor model contains essential information, we compared our correction model’s results with and without the latent confounder, as shown in Table 3. The performance improved significantly with the inclusion of the hidden confounder.

Conclusion

In this paper, we proposed the deconfounding bias correction method, with the presence of multi-cause confounders. By integrating climate bias correction techniques with advancements in causality based time series deconfounding method, our approach offers a novel perspective for future studies. This highlights the importance of not always assuming that all variables are observed.

References

- Bi, K.; Xie, L.; Zhang, H.; Chen, X.; Gu, X.; and Tian, Q. 2023. Accurate medium-range global weather forecasting with 3D neural networks. *Nature*, 619(7970): 533–538.
- Bica, I.; Alaa, A. M.; and van der Schaar, M. 2020. Time Series Deconfounder: Estimating Treatment Effects over Time in the Presence of Hidden Confounders. arXiv:1902.00450.
- Cannon, A. J.; Sobie, S. R.; and Murdock, T. Q. 2015. Bias Correction of GCM Precipitation by Quantile Mapping: How Well Do Methods Preserve Changes in Quantiles and Extremes? *Journal of Climate*, 28(17): 6938–6959.
- Casanueva, A.; Herrera, S.; Iturbide, M.; Lange, S.; Jury, M.; and Dosio, A. 2020. Testing bias adjustment methods for regional climate change applications under observational uncertainty and resolution mismatch. *Atmospheric Science Letters*, 21: 1–12.
- Chen, J.; Brissette, F.; Chaumont, D.; and Braun, M. 2013. Finding appropriate bias correction methods in downscaling precipitation for hydrologic impact studies over North America. *Water Resources Research*, 49: 4187–4205.
- Cheng, D.; Xu, Z.; Li, J.; Liu, L.; Liu, J.; Gao, W.; and Le, T. D. 2023. Instrumental Variable Estimation for Causal Inference in Longitudinal Data with Time-Dependent Latent Confounders. arXiv:2312.07175.
- Dowdy, A. 2020. Seamless climate change projections and seasonal predictions for bushfires in Australia. *Journal of Southern Hemisphere Earth Systems Science*, 70: 120–138.
- Enayati, M.; Bozorg-Haddad, O.; Bazrafshan, J.; Hejabi, S.; and Chu, X. 2020. Bias correction capabilities of quantile mapping methods for rainfall and temperature variables. *Journal of Water and Climate Change*, 12: 401–419.
- Eyring, V.; Bony, S.; Meehl, G. A.; Senior, C. A.; Stevens, B.; Stouffer, R. J.; and Taylor, K. E. 2016. Overview of the Coupled Model Intercomparison Project Phase 6 (CMIP6) experimental design and organization. Geoscientific Model Development.
- Feigenwinter, I.; Kotlarski, S.; Casanueva, A.; Schwierz, C.; and Liniger, M. 2018. Exploring quantile mapping as a tool to produce user-tailored climate scenarios for Switzerland. *Technical Report MeteoSwiss*, 270: 44.
- Heo, J.; Kim, D.; Seo, Y.; Nam, W.; and Shin, J. 2019. A Bayesian framework for quantile mapping to correct systematic bias in climate model outputs. *Water Resources Research*, 55: 1371–1391.
- Huang, Y.; Hall, A.; and Berg, N. 2014. Quantile mapping for spatial disaggregation of precipitation extremes in the United States. *Journal of Hydrometeorology*, 15(3): 1050–1067.
- Lafferty, D. C.; and Srivier, R. L. 2023. Downscaling and bias-correction contribute considerable uncertainty to local climate projections in CMIP6. *npj Climate and Atmospheric Science*, 6(1): 158.
- Lafon, T.; Dadson, S.; Buys, G.; and Prudhomme, C. 2013. Bias correction of daily precipitation simulated by a regional climate model: a comparison of methods. *International Journal of Climatology*, 33: 1367–1381.
- Li, Z.; Shen, Y.; Zheng, K.; Cai, R.; Song, X.; Gong, M.; Zhu, Z.; Chen, G.; and Zhang, K. 2024. On the Identification of Temporally Causal Representation with Instantaneous Dependence. arXiv:2405.15325.
- Liu, Y.; Hu, T.; Zhang, H.; Wu, H.; Wang, S.; Ma, L.; and Long, M. 2024. iTransformer: Inverted Transformers Are Effective for Time Series Forecasting. arXiv:2310.06625.
- Maraun, D. 2016. Bias correcting climate change simulations—a critical review. *Current Climate Change Reports*, 2: 211–220.
- Maraun, D.; and Widmann, M. 2018. *Statistical Downscaling and Bias Correction for Climate Research*. Cambridge University Press.
- Mehrotra, R.; Johnson, F.; and Sharma, A. 2018. A software toolkit for correcting systematic biases in climate model simulations. *Environmental Modelling & Software*, 104: 130–152.
- Miao, C.; Su, L.; Sun, Q.; and Duan, Q. 2016. A nonstationary bias-correction technique to remove bias in GCM simulations. *Journal of Geophysical Research: Atmospheres*, 121: 5718–5735.
- Mouatadid, S.; Orenstein, P.; Flaspohler, G.; et al. 2023. Adaptive bias correction for improved subseasonal forecasting. *Nature Communications*, 14: 3482. Received: 23 September 2022; Accepted: 15 May 2023; Published: 15 June 2023.
- Nahar, J.; Johnson, F.; and Sharma, A. 2018. Addressing spatial dependence bias in climate model simulations—an independent component analysis approach. *Water Resources Research*, 54: 827–841.
- Nivron, O.; Wischik, D. J.; Vrac, M.; Shuckburgh, E.; and Archibald, A. T. 2024. A Temporal Stochastic Bias Correction using a Machine Learning Attention model. arXiv:2402.14169.
- Pastén-Zapata, E.; Jones, J.; Moggridge, H.; and Widmann, M. 2020. Evaluation of the performance of Euro-CORDEX regional climate models for assessing hydrological climate change impacts in Great Britain: a comparison of different spatial resolutions and quantile mapping bias correction methods. *Journal of Hydrology*, 584: 124653.
- Pearl, J. 2000. *Causality: Models, Reasoning, and Inference*. New York, NY, USA: Cambridge University Press.
- Pearl, J. 2009. *Causality: Models, Reasoning, and Inference*. New York: Cambridge University Press, 2nd edition.
- Piani, C.; Haerter, J.; and Coppola, E. 2010. Statistical bias correction for daily precipitation in regional climate models over Europe. *Theoretical and Applied Climatology*, 99: 187–192.
- Rubin, D. B. 1974. Estimating causal effects of treatments in randomized and nonrandomized studies. *Journal of Educational Psychology*, 66(5): 688–701.
- Smitha, P.; Narasimhan, B.; Sudheer, K.; and Annamalai, H. 2018. An improved bias correction method of daily rainfall data using a sliding window technique for climate change impact assessment. *Journal of Hydrology*, 556: 100–118.

Teutschbein, C.; and Seibert, J. 2012a. Bias correction of regional climate model simulations for hydrological climate-change impact studies: Review and evaluation of different methods. *Journal of Hydrology*, 456: 12–29.

Teutschbein, C.; and Seibert, J. 2012b. Bias correction of regional climate model simulations for hydrological climate-change impact studies: Review and evaluation of different methods. *Journal of Hydrology*, 456-457: 12–29.

Tong, Y.; Gao, X.; Han, Z.; et al. 2021. Bias correction of temperature and precipitation over China for RCM simulations using the QM and QDM methods. *Climate Dynamics*, 57: 1425–1443.

Wang, S.; Wu, H.; Shi, X.; Hu, T.; Luo, H.; Ma, L.; Zhang, J. Y.; and ZHOU, J. 2024. TimeMixer: Decomposable Multiscale Mixing for Time Series Forecasting. In *International Conference on Learning Representations (ICLR)*.

Wang, Y.; and Blei, D. M. 2019. The blessings of multiple causes. *Journal of the American Statistical Association*, 1–71. Just-accepted.

Wu, H.; Hu, T.; Liu, Y.; Zhou, H.; Wang, J.; and Long, M. 2023a. TimesNet: Temporal 2D-Variation Modeling for General Time Series Analysis. arXiv:2210.02186.

Wu, H.; Xu, J.; Wang, J.; and Long, M. 2022a. Autoformer: Decomposition Transformers with Auto-Correlation for Long-Term Series Forecasting. arXiv:2106.13008.

Wu, H.; Zhou, H.; Long, M.; and Wang, J. 2023b. Interpretable weather forecasting for worldwide stations with a unified deep model. *Nature Machine Intelligence*, 5: 602–611.

Wu, Y.; Miao, C.; Fan, X.; Gou, J.; Zhang, Q.; and Zheng, H. 2022b. Quantifying the uncertainty sources of future climate projections and narrowing uncertainties with bias correction techniques. *Earth's Future*, 10: e2022EF002963.

Xu, Z.; Cheng, D.; Li, J.; Liu, J.; Liu, L.; and Wang, K. 2023. Disentangled Representation for Causal Mediation Analysis. *Proceedings of the AAAI Conference on Artificial Intelligence*, 37(9): 10666–10674.

Zhou, H.; Zhang, S.; Peng, J.; Zhang, S.; Li, J.; Xiong, H.; and Zhang, W. 2021. Informer: Beyond Efficient Transformer for Long Sequence Time-Series Forecasting. arXiv:2012.07436.